

1 **Production of π^+ and K^+ mesons in 3.2 AGeV**
2 **argon-nucleus interactions at the Nuclotron**

3 **BM@N Collaboration**

4 **Abstract**

5 First physics results of the BM@N experiment are presented on π^+ and K^+
6 meson production in interactions of the 3.2 AGeV argon beam with fixed
7 targets. Transverse momentum, rapidity spectra and multiplicities of π^+
8 and K^+ mesons are measured. The results are compared with predictions of
9 theoretical models and with the measurements from heavy ion experiments
10 at lower energies.

1 Introduction

BM@N (baryonic matter at Nuclotron) is the first experiment operational at the ion-accelerating complex Nuclotron/NICA, studying interactions of relativistic beams of heavy ions with fixed targets [1] in the energy range of high densities of baryons [2]. At the Nuclotron energies, the density of nucleons in a fireball created by two colliding heavy nuclei is 3-4 times higher than the saturation density [3]. In addition, these energies are high enough to study strange mesons and (multi)-strange hyperons produced in nucleus-nucleus collisions close to the kinematic threshold [4, 5]. The primary goal of the experiment is to constrain parameters of the equation of state (EoS) of high-density nuclear matter. Studies of the excitation function of strange particle production below and near to the kinematical threshold make it possible to distinguish hard behaviour of the EoS from the soft one [6].

The Nuclotron will provide the experiment with beams of a variety of particles, from protons to gold ions, with kinetic energy in the range from 1 to 6 GeV/nucleon for light ions with Z/A ratio of ~ 0.5 and up to 4.5 GeV/nucleon for heavy ions with Z/A ratio of ~ 0.4 .

Recently BM@N collected first experimental data in beams of carbon, argon, and krypton ions [7, 8]. This paper presents first results on π^+ and K^+ meson production in 3.2 AGeV argon-nucleus interactions. The experimental data correspond to an integrated luminosity of $7.8 \mu\text{b}^{-1}$ collected with different targets: $2.1 \mu\text{b}^{-1}$ (carbon), $2.3 \mu\text{b}^{-1}$ (Al), $1.8 \mu\text{b}^{-1}$ (Cu), $1.1 \mu\text{b}^{-1}$ (Sn), $0.5 \mu\text{b}^{-1}$ (Pb).

The paper is organized as follows. Section 2 describes the experimental set-up and section 3 is devoted to details of the event reconstruction. Section 4 describes the evaluation of the π^+ , K^+ reconstruction efficiency. Experimental results on transverse momentum, rapidity spectra and multiplicities of π^+ and K^+ mesons are given in section 5. The BM@N measurements are compared with predictions of theoretical models and with experimental data on medium-sized nucleus-nucleus interactions measured at lower energies. Finally, the results are summarized in section 6.

2 Experimental set-up

The BM@N detector is a forward spectrometer covering the pseudorapidity range $1.6 \leq \eta \leq 4.4$. Schematic view of the BM@N setup in the argon-beam run is shown in figure 1. Components of the set-up are described in [9]. The spectrom-

45 eter includes a central tracking system consisting of 3 planes of forward silicon-
 46 strip detectors (ST) and 6 planes of detectors based on gas electron multipliers
 47 (GEM) [10]. The central tracking system is located downstream of the target re-
 48 gion inside of a dipole magnet with the bending power of about $\approx 2.1\text{Tm}$.

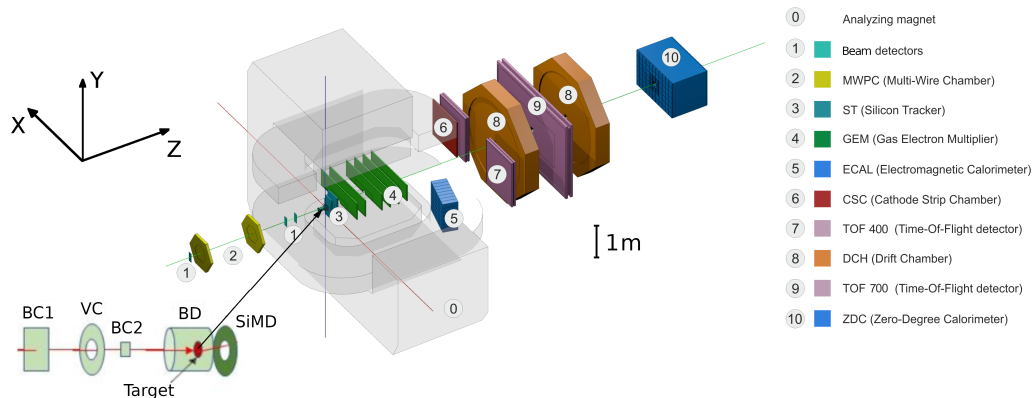


Figure 1: Schematic view of the BM@N setup in the argon-beam run.

49 Outer drift chambers (DCH), a cathode strip chamber (CSC), two sets of time-
 50 of-flight detectors (ToF) and a zero degree calorimeter (ZDC) are located down-
 51 stream the dipole magnet. The tracking system measures of momenta, p , of
 52 charged particles with a relative uncertainty that varies from 2.5% at the momen-
 tum of 0.5 GeV/c to 4.5% at 3.5 GeV/c as it is shown in figure 2.

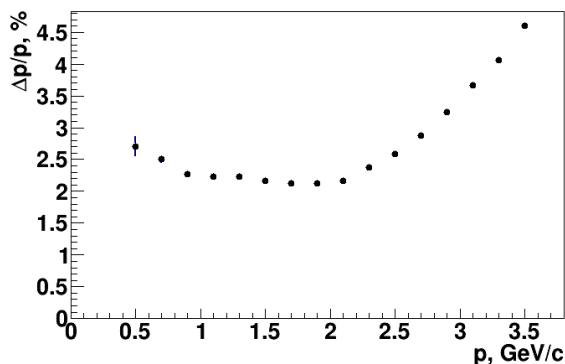


Figure 2: Relative momentum resolution as a function of the momentum.

53
 54 The primary collision vertex position (PV) is measured with a resolution of 2.4
 55 mm in the X-Y plane and in the beam direction at the target position. The dis-

56 tribution of the primary vertices along the beam direction (Z_{ver}) for experimental
57 data and Monte Carlo events is shown in figure 7e. Two vertical lines limit the re-
58 gion of the Z coordinate accepted for the data analysis for all the targets. Different
59 types of charged hadrons are identified by two ToF systems.

60 The event triggering is performed by a trigger, based on two beam counters
61 (BC1, BC2), a veto counter (VC), a barrel detector (BD) and a silicon multiplicity
62 detector (SiMD). The BC2 counter was used as a start trigger T0. The BD de-
63 tector consists of 40 azimuthal scintillating strips arranged around the target, and
64 the SiMD detector consists of 60 azimuthal silicon segments situated behind the
65 target.

66 To count the number of beam ions that passed through the target, a logical
67 beam trigger $BT = BC1 \otimes \overline{VC} \otimes BC2$ was used. The following logic conditions
68 were applied to generate the trigger signal: 1) $BT \otimes (BD \geq 4)$; 2) $BT \otimes (SiMD \geq 4)$;
69 3) $BT \otimes (BD \geq 2) \otimes (SiMD \geq 3)$. The trigger conditions were varied to find the op-
70 timal ratio between the event rate and the trigger efficiency for each target. Trigger
71 condition 1 was applied for 60% of data collected with the carbon target. This trig-
72 ger fraction was continuously reduced with the atomic weight of the target down
73 to 26% for the Pb target. The fraction of data collected with trigger condition 2
74 was rising from 6% for the carbon target up to 34% for the Pb target. The rest of
75 data were collected with trigger condition 3. The measurements cover the entire
76 range of event centralities, but the trigger efficiency was lower for peripheral in-
77 teractions than for central and semi-central collisions (see figure 9 in section 4)

78 .
79 The data from the forward silicon detectors, GEM detectors, outer drift chambers,
80 cathode strip chamber and two sets of the time-of-flight detectors ToF-400 and
81 ToF-700 were used for the analysis. The acceptances of the ToF-400 [33] and ToF-
82 700 [34] detectors cover different ranges of the rapidity and transverse momentum
83 of detected particles. The time resolutions of the ToF-400 and ToF-700 systems
84 are 84 ps and 115 ps, respectively [35]. For argon-nucleus collisions at 3.2 AGeV,
85 83M events were analysed.

86 The research program of the run was devoted to measurements of inelastic
87 reactions $Ar + A \rightarrow X$ with the argon beam intensity of a few 10^5 ions per spill
88 and a spill duration of 2–2.5 sec. A set of 3% nuclear length solid targets of
89 various materials (C, Al, Cu, Sn, Pb) was used.

3 Event reconstruction

Track reconstruction in the central tracker is based on a “cellular automaton” approach [11] implementing a constrained combinatorial search of track candidates with their subsequent fitting by the Kalman filter to determine track parameters. These tracks are used to reconstruct primary (interaction) and secondary (decay) vertices and global tracks by extrapolation to the downstream detectors (CSC, DCH and ToF) and matching with their measurements.

Charged mesons (π^+ and K^+) were identified using the time of flight measured in T0 and ToF detectors, the length of the trajectory and the momentum reconstructed in the central tracker. Candidates to π^+ and K^+ must originate from the primary vertex and match hits in CSC and ToF400 or in the DCH and ToF-700 detectors.

The criteria for selecting of π^+ and K^+ meson candidates were the following:

- Each track has at least 4 hits in the GEM detectors (6 detectors in total) [10]. Hits in the forward silicon detectors were used to reconstruct the track, but no requirements were applied to the number of hits;
- Tracks originate from the primary vertex, the deviation of the reconstructed vertex from the target position along the beam direction is limited to $-3.4 \text{ cm} < Z_{\text{ver}} - Z_0 < 1.7 \text{ cm}$, where Z_0 is the target position. The upper limit corresponds to 7σ of the Z_{ver} spread and cuts off interactions with the trigger detector located at 3 cm behind the target (see figure 7e);
- Distance from a track to the primary vertex in the X-Y plane at Z_{ver} (DCA) is required to be less than 1 cm, which corresponds to 4σ of the vertex resolution in the X-Y plane;
- Momentum range of positively charged particles $p > 0.5, 0.7 \text{ GeV}/c$ is limited by the acceptance of the ToF-400 and ToF-700 detectors, respectively;
- Distance of extrapolated tracks to the CSC (DCH) hits as well as to the ToF-400 (ToF-700) hits should be within $\pm 2.5\sigma$ of the hit-track residual distributions and depends upon the track momentum range as shown in figure 3.

The spectra of the mass squared (M^2) of positively charged particles produced in interactions of the 3.2 AGeV argon beam with various targets are shown in figures 4a and 4b for ToF-400 and ToF-700 data, respectively. The π^+ and

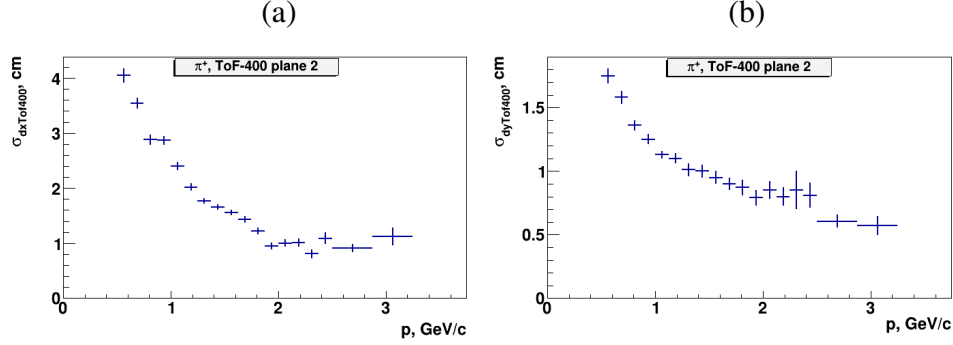


Figure 3: Sigma of the Gaussian fit of the ToF-400 hit residuals with respect to positively charged tracks depending on the particle momentum: projection X (a), Y (b).

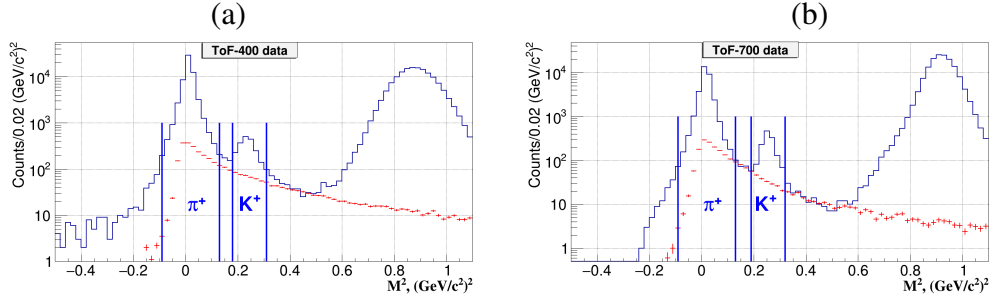


Figure 4: M^2 spectra of positively charged particles produced in argon-nucleus interactions and measured in the ToF-400 (a) and ToF-700 (b) detectors. Vertical lines show the signal ranges of the identified π^+ and K^+ mesons. Red points with error bars show the the background estimated from "mixed events".

123 K^+ signals were extracted in the M^2 windows from -0.09 to 0.13 (GeV/c) 2 ²
 124 and from 0.18 to 0.32 (GeV/c) 2 ², respectively. The signals of π^+ and K^+ and
 125 statistical errors were calculated according to the formulae: $sig = hist - bg$,
 126 $err_{stat} = \sqrt{hist + bg}$, assuming the background uncertainty of \sqrt{bg} . Here $hist$
 127 and bg denote the histogram integral and the background integral within the M^2
 128 windows of π^+ and K^+ mesons.

129 To estimate the background under the π^+ and K^+ signals, the "mixed event"
 130 method was used, i.e. the shape of the M^2 background distribution was estimated
 131 by matching tracks to hits in the ToF-400 and ToF-700 detectors taken from inde-
 132 pendent events. To estimate the systematic errors of the π^+ and K^+ signals due
 133 to the background subtraction method, the M^2 distributions were parameterised
 134 using a linear fit in the M^2 range -0.14-0.4 (GeV/c) 2 ². The M^2 windows of the

135 π^+ and K^+ signals were excluded from the linear fit. The difference between the
 136 background integral under the π^+ and K^+ signals taken from “mixed events” and
 137 the bg integral taken from the fitting of the M^2 spectra was treated as a systematic
 138 error.

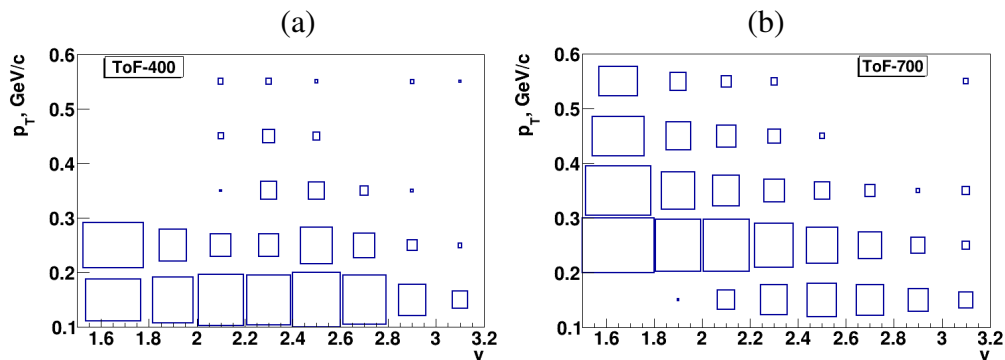


Figure 5: Distribution of the π^+ signals measured in ToF-400 (a) and ToF-700 (b) in the rapidity and transverse momentum bins in Ar+Sn interactions.

139 The fraction of fake combinations of tracks and hits in the ToF detectors was
 140 estimated by the “mixed event” method described above. It was found that this
 141 fraction differs when the beam interacts with with light and heavy targets and for
 142 different intervals of the rapidity and transverse momentum.

143 Figure 5 shows coverage of the phase space of the π^+ signals measured in
 144 ToF-400 and ToF-700 in the rapidity and transverse momentum intervals in Ar+Sn
 145 interactions before making corrections for the efficiency.

146 4 Reconstruction and trigger efficiency

147 Monte Carlo data samples of argon-nucleus collisions were produced with the
 148 DCM-SMM event generator [12, 13]. Propagation of particles through the entire
 149 detector volume and responses of the detectors were simulated using the GEANT3
 150 program [14] integrated into the BmnRoot software framework [15]. To properly
 151 describe the GEM detector response in the magnetic field, the Garfield++ toolkit
 152 [16] for simulation of the micropattern gaseous detectors was used.

153 The efficiencies of the forward silicon, GEM, CSC, DCH and ToF detectors
 154 were adjusted during simulation in accordance with the detector efficiencies mea-
 155 sured in the experimental events. The Monte Carlo events went through the same
 156 chain of reconstruction and identification as the experimental events.

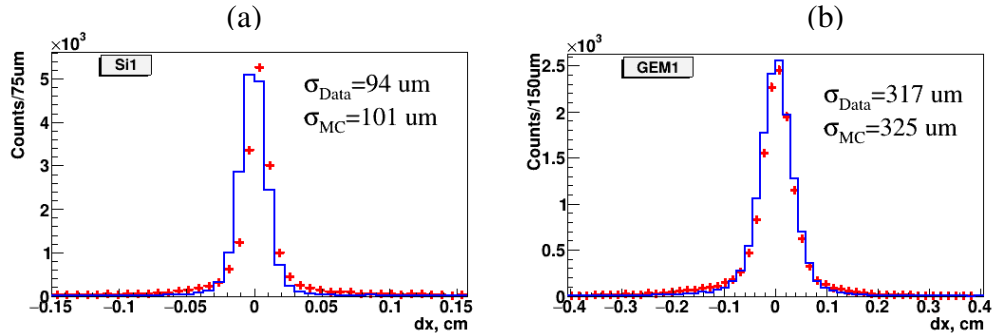


Figure 6: Residual distributions of hits in the X projection (magnet deflection plane) with respect to reconstructed tracks: (a) - in the first forward silicon plane, (b) - in the first GEM plane. The experimental data are shown as red crosses, and the simulated data are shown as blue histograms.

157 The level of agreement between the Monte Carlo and experimental distribu-
 158 tions is demonstrated on a set of observables: hit-track residuals in the central
 159 tracker detectors, DCA, χ^2/NDF , number of tracks reconstructed at the primary
 160 vertex and number of hits per track (see figures 6 and 7a-d).

161 The π^+ and K^+ reconstruction efficiency is estimated in the intervals of ra-
 162 pidity y and transverse momentum p_T . It takes into account the geometrical ac-
 163 ceptance, the detector efficiency, the kinematic and spatial cuts efficiency and loss
 164 of π^+ and K^+ due to decays on the fly. The reconstruction efficiencies of π^+
 165 detected in ToF-400 and ToF-700 are shown in figure 8 in the y and p_T intervals
 166 for Ar+Sn interactions.

167 The efficiency to get a trigger signal based on multiplicities of fired channels
 168 in the BD (SiMD) detectors ϵ_{trig} was calculated using experimental event samples
 169 recorded with an independent trigger based on the SiMD (BD) detectors: ϵ_{trig}
 170 $(\text{BD} \geq m) = N(\text{BD} \geq m, \text{SiMD} \geq n) / N(\text{SiMD} \geq n)$, where m and n are the
 171 minimum number of fired channels in BD and SiMD varied in the range from
 172 2 to 4. The dependences of the trigger efficiency on the track multiplicity in
 173 the primary vertex and the X/Y vertex position were taken into account. The
 174 efficiency for combined BD and SiMD triggers was calculated as the product of
 175 the efficiencies of BD and SiMD triggers. The systematic errors estimated in
 176 the analysis cover variations in the trigger efficiency as a function of the number
 177 of on-vertex tracks and position of the primary vertex relative to the mean value
 178 of trigger efficiency. The trigger efficiency averaged over all data collected with
 179 the trigger conditions 1) $\text{BD} \geq 4$; 2) $\text{SiMD} \geq 4$; 3) $(\text{BD} \geq 2) \otimes (\text{SiMD} \geq 3)$ (see

180 section 2) is shown in Fig.9 as a function of the event centrality estimated from
 181 the simulation.

182 5 Results

183 The differential cross sections $d^2\sigma_{\pi,K}(y, p_T)/dydp_T$ and yields $d^2N_{\pi,K}(y, p_T)/dydp_T$
 184 of π^+ and K^+ meson production in Ar+C, Al, Cu, Sn, Pb interactions are calcu-
 185 lated in bins of (y, p_T) by the formulas:

$$186 \quad d^2\sigma_{\pi,K}(y, p_T)/dydp_T = n_{\pi,K}(y, p_T)/(\epsilon_{rec}(y, p_T)\epsilon_{trig}Ldydp_T)$$

$$187 \quad d^2N_{\pi,K}(y, p_T)/dydp_T = d^2\sigma_{\pi,K}(y, p_T)/(\sigma_{inel}dydp_T) \quad (1)$$

188 where L is the luminosity, $n_{\pi,K}$ is the number of reconstructed π^+ and K^+ mesons
 189 in intervals dy and dp_T , ϵ_{rec} is the efficiency of the π^+ and K^+ meson recon-
 190 struction, ϵ_{trig} is the trigger efficiency, σ_{inel} is the cross section for the mini-
 191 mum bias inelastic argon-nucleus interactions. The cross sections for inelastic
 192 Ar+C, Al, Cu, Sn, Pb interactions are taken from the predictions of the DCM-
 193 SMM model which are consistent with the results calculated by the formula:
 194 $\sigma_{inel} = \pi R_0^2(A_P^{1/3} + A_T^{1/3})^2$, where $R_0 = 1.2$ fm is the effective nucleon radius, A_P
 195 and A_T are the atomic numbers of the projectile and target nucleus [29]. The un-
 196 certainties for the Ar+C, Al, Cu, Sn, Pb inelastic cross sections are estimated from
 197 an alternative formula ([20]) which approximates the measured nucleus-nucleus
 198 cross sections: $\sigma_{inel} = \pi R_0^2(A_P^{1/3} + A_T^{1/3} - b)^2$ with $R_0 = 1.46$ fm and $b = 1.21$
 199 The values and uncertainties of σ_{inel} for Ar+C, Al, Cu, Sn, Pb interactions used
 200 to estimate the yields of π^+ and K^+ mesons are given in table 2.

201 The yields of π^+ (K^+) mesons in Ar+C, Al, Cu, Sn, Pb interactions are mea-
 202 sured in the kinematic range of the transverse momentum of π^+ (K^+) meson
 203 $0.1 < p_T < 0.6$ GeV/c ($0.1 < p_T < 0.5$ GeV/c) and the π^+ (K^+) meson rapidity
 204 in the laboratory frame $1.5 < y < 3.2$ ($1.0 < y < 2.0$). The systematic error of
 205 the π^+ and K^+ meson yield in each p_T and y bin is calculated as the quadratic
 206 sum of the uncertainties coming from the following sources:

- 207 • Sys1: systematic errors of the reconstruction efficiency due to the remain-
 208 ing difference in the X/Y distribution of primary vertices in the simulation
 209 relative to experimental data.
- 210 • Sys2: systematic errors of the background subtraction under the π^+ and
 211 K^+ signals in the mass-squared spectra of identified particles as described
 212 in section 3. This uncertainty affects the number of reconstructed π^+ and

213 K^+ in p_T and y bins in data as well as in simulated events. As a result its
214 effect is smaller for the π^+ and K^+ yields calculated by formula (1).

- 215 • Sys3: systematic error of the trigger efficiency estimated as a function of the
216 number of tracks from the primary vertex and the X/Y position of primary
217 vertex.

218 In addition to uncertainties Sys1-Sys3, uncertainties of the normalization of the
219 π^+ and K^+ yields were estimated. The normalization uncertainties are treated
220 as fully correlated in all bins of y and p_T . The π^+ and K^+ meson yield normal-
221 ization uncertainties are calculated for the entire measured (y, p_T) range as the
222 quadratic sum of the statistical uncertainty of the trigger efficiency, uncertainties
223 of the tracking detector efficiency, efficiency of the track matching to the CSC
224 (DCH) outer detectors and to ToF-400 (ToF-700), uncertainties of the luminosity
225 and inelastic nucleus-nucleus cross section. The luminosity uncertainty is esti-
226 mated to be within 2%. It corresponds to the fraction of the beam which can miss
227 the target, estimated from the vertex positions of the data. The statistical uncer-
228 tainty of the trigger efficiency is 28% for detecting K^+ in Ar+C interactions and
229 between 7.5% (Ar+Al) and 4% (Ar+Pb) for detecting K^+ in interactions of argon
230 ions with heavier targets. The statistical uncertainty of the trigger efficiency for
231 the π^+ detection ranges between 4.5% (Ar+C) and 0.9% (Ar+Pb). The uncer-
232 tainty of the central tracking detector efficiency is estimated to be within 3%. Its
233 effect is estimated from the remaining difference in the number of track hits in the
234 central detectors in the simulation relative to the experimental data (see figure 7d).
235 The combined uncertainty of matching of extrapolated tracks to the CSC (DCH)
236 hits and ToF-400 (ToF-700) hits is within 5%. It is estimated from the remaining
237 difference in the matching efficiency in the simulation relative to the experimental
238 data. Table 1 summarizes the total systematic uncertainty arized from the sources
239 Sis1 - Sis3 and the uncertainty of normalization of the π^+ and K^+ yields.

240 The differential y spectra of the π^+ and K^+ meson yields are calculated in the
241 p_T bins using formulae (1) and are shown in figures 10 and 11, respectively. The
242 measurements correspond to the forward and central rapidity range in the nucleon-
243 nucleon CM system because the rapidity of the beam-target nucleon-nucleon CM
244 system is $y_{CM} = 1.08$ for the 3.2 GeV/nucleon beam kinetic energy. Predictions
245 of the DCM-SMM [12, 13], UrQMD [18] and PHSD [19] models are shown for
246 comparison. Although the DCM-SMM model was used to estimate the recon-
247 struction efficiency (section 4), model's predictions as such, may well differ from
248 the measurement results. All three models predict a flatter behaviour of the π^+
249 spectra as a function of rapidity at low p_T compared to with the experiment. The

250 experimental spectra of π^+ are 1.5 times lower than the model predictions for
 251 the production of π^+ in Ar+C interactions. This result can be tested in the fu-
 252 ture with other targets with low atomic weight. All three models predict higher
 253 multiplicities of K^+ at low p_T than those measured in the experiment. But the
 254 difference is smaller at larger values of p_T . The DCM-SMM model predicts a
 255 higher K^+ multiplicity at low p_T and rapidity compared to PHSD, whereas the
 256 UrQMD predictions are lower than PHSD at low p_T . The p_T spectra of π^+ and
 257 K^+ mesons are measured in the bins of rapidity y and are shown in figures 12 and
 258 13, respectively. Due to low statistics of the K^+ meson signal in Ar+C interac-
 259 tions, the results are given only for the entire measured range in y and p_T . The
 260 p_T spectra of K^+ mesons over the entire measured rapidity range are shown in
 261 figure 14. In figures 12, 13 and 14 the measured p_T spectra of π^+ and K^+ mesons
 262 are parameterised by the form:

$$263 \quad 1/p_T \cdot d^2N/dydp_T \propto \exp(-(m_T - m_{\pi,K})/T_0),$$

264 where $m_T = \sqrt{m_{\pi,K}^2 + p_T^2}$ is the transverse mass, dy is the width of y bin, dp_T is
 265 the width of p_T bin, the inverse slope parameter T_0 – free fitting parameter. The
 266 values of the inverse slope T_0 , determined from the fits of the p_T spectra of π^+ and
 267 K^+ mesons are given in figures 15 and 16, respectively. The value of T_0 measured
 268 for π^+ mesons produced in argon-nucleus interactions at the 3.2 AGeV beam ki-
 269 netic energy of is about 40 MeV in the forward rapidity range, rising to 90 MeV
 270 in the central rapidity range. In general, the y dependence of the fitting results
 271 for π^+ mesons is consistent with the predictions of the DCM-SMM, UrQMD and

Table 1: Systematic uncertainties of the π^+ and K^+ yields measured in argon-nucleus interactions.

Systematics	Reaction	Ar+C sys%	Ar+Al sys%	Ar+Cu sys%	Ar+Sn sys%	Ar+Pb sys%
Sys1, π^+		7	6	6	4	4
Sys2, π^+		11	8	9	7	7
Sys3, π^+		7	7	7	7	7
Norm (trigger + tracking + luminosity), π^+		7.8	6.3	6.2	6.2	6.2
Sys1, K^+		15	14	7	7	9
Sys2, K^+		19	18	11	9	11
Sys3, K^+		14	12	7	7	7
Norm (trigger + tracking + luminosity), K^+		29	10	8.4	7.6	7.4

272 PHSD models, but the results of BM@N measurements give a flatter dependence
 273 of the T_0 values in the central rapidity range compared to the rising dependence
 274 of the inverse slopes predicted by the models. The T_0 values measured in 3 y bins
 275 for K^+ mesons have large statistical and systematic errors (see figure 16), but the
 276 slope dependence on y is rather weak. The T_0 values obtained for the entire mea-
 277 sured range of $1.0 < y < 2.0$ are consistent within the errors with 80 MeV for
 278 all the targets (see table 3). The weak dependence of the slope T_0 is reproduced
 279 by all three models, but UrQMD predicts 2 times larger values compared to the
 280 measurement. Measured values of π^+ and K^+ meson multiplicities in the inter-
 281 actions of Ar+C, Al, Cu, Sn, Pb are extrapolated to the entire kinematic range
 282 using the averaged values of the extrapolation coefficients from the predictions
 283 of the DCM-SMM, UrQMD and PHSD models which are shown in table 2. The
 284 maximal differences of the predictions of the models from the averaged values are
 285 taken as the uncertainties of the extrapolation coefficients. The multiplicities of
 286 K^+ and π^+ mesons and their ratios are summarized in table 3. The ratios of the
 287 K^+ to π^+ multiplicities do not show a significant dependence on the mean number
 288 of participant nucleons, A_{part} , in argon-nucleus collisions shown in table 2. The
 289 values of A_{part} are calculated based on the predictions of the DCM-SMM model.

290 The results of BM@N on the π^+ and K^+ multiplicities are compared with
 291 predictions of the DCM-SMM, UrQMD and PHSD models in figures 17a,b. The
 292 measured ratios of the π^+ and K^+ meson multiplicities to A_{part} decrease with the
 293 increasing atomic weight of the target from Al to Pb. The result for π^+ in Ar+C
 294 interactions is below the results for heavier targets. The ratios of the K^+ to π^+
 295 multiplicities are given in figure 17c. They show no dependence on the number of
 296 participant nucleons. The PHSD prediction is compatible with this result, whereas
 297 the DCM-SMM and UrQMD models predict smooth rising of the K^+ to π^+ ratio
 298 with A_{part} .

299 The π^+ and K^+ meson multiplicities in argon-nucleus interactions can be
 300 compared with the previous results of the HADES experiment measured Ar+KCl
 301 interactions at the lower beam kinetic energy of 1.76 AGeV [21–23] and with
 302 the FOPI experiment, in which Ni+Ni interactions were measured at the beam
 303 kinetic energy of 1.93 AGeV [24–26]. The KaoS experiment also measured the
 304 K^+ multiplicities in Ni+Ni interactions at the beam kinetic energies of 1.5 and
 305 1.93 AGeV [27, 28] which are consistent with the results of the FOPI experiment.
 306 The HADES experiment measured the total multiplicities of π^- and K^+ in semi-
 307 central events (the mean number of participant nucleons A_{part} is 38.5) of 3.9 and
 308 $2.8 \cdot 10^{-2}$, respectively. The effective inverse slope parameters of the m_T spectra
 309 of π^- and K^+ extrapolated to $y^* = 0$ are 82.4 MeV and 89 MeV, respectively.

310 The BM@N results on the K^+ and π^+ multiplicities at the beam kinetic energy
 311 of 3.2 AGeV in Ar+Cu interactions (A_{part} of 33.6, see table 2) are higher by factors
 312 of 5 and 1.3 relative to the results for kaons and pions measured by HADES.
 313 The difference in the K^+ multiplicities could be explained by the energy dependence
 314 of the K^+ cross section near the kinematical threshold for K^+ production
 315 ($E_{thr}(NN) \sim 1.58$ GeV). The inverse slope parameters T_0 measured for π^+ and
 316 K^+ in the central rapidity range (see figures 15 and 16) are comparable to the
 317 HADES results.

318 The FOPI experiment measured the total multiplicities of K^+ in triggered
 319 semi-central Ni+Ni interactions (A_{part} of 46.5) and central events (A_{part} of 75) of
 320 $3.6 \cdot 10^{-2}$ and $8.25 \cdot 10^{-2}$, respectively. These values can be compared with the
 321 BM@N results presented in table 3 for various targets. The K^+/π^+ multiplicity
 322 ratio measured by FOPI in triggered semi-central events is $7.6 \cdot 10^{-3}$, which is by
 323 a factor 3 smaller than the K^+/π^+ multiplicity ratio obtained by BM@N in Ar
 324 + Sn interactions for the entire kinematical range (A_{part} of 48.3, see table 2). It
 325 should be taken into account that the beam kinetic energy of the FOPI experiment
 326 (1.93 AGeV) is lower than that of the BM@N experiment. The effective inverse
 327 slope of 110.9 MeV, estimated by FOPI at $y^* = 0$ from the K^+ transverse mass
 328 spectrum is consistent within the uncertainties with the inverse slope parameter
 329 T_0 , measured by BM@N for K^+ in the range $y^* \gtrsim 0$. The consistency of the
 330 transverse momentum slopes measured by BM@N with the results of the HADES
 331 and FOPI experiments indicates the absence of a strong dependence on the
 332 beam energy and atomic weights of colliding nuclei.

333 Multiplicities of pions in the entire kinematic range N_{π}^{tot} , where $N_{\pi}^{tot} = N_{\pi^+}^{tot} +$
 334 $N_{\pi^-}^{tot} + N_{\pi^0}^{tot}$, normalized to the average number of participant nucleons A_{part} are
 335 compiled in figure 18 for different colliding nuclei and beam energies. Reference [36]
 336 contains compilation of the pion data for interactions of nucleon-nucleon (N+N) [38],
 337 Mg+Mg [39], La+La [40], Au+Au [41–43], Ar+KCl [44], Si+Al, S+S [45, 46],
 338 Pb+Pb [47, 55]. The reference [37] compiles the pion data for Au+Au [48–51].
 339 To estimate N_{π}^{tot} from the π^+ multiplicities measured by BM@N, the predictions
 340 of the DCM-SMM model are used. Multiplicities of K^+ in the entire kinematic
 341 range normalized to the average number of participant nucleons A_{part} are
 342 compiled in figure 19. The world data taken from [24, 52–55] are compared with
 343 the results of the BM@N experiment. Figures 18 and 19 show that the BM@N
 344 results are consistent with the world data on the production of π and K^+ .
 345

346 **6 Summary**

347 First physics results of the BM@N experiment are presented on the π^+ and K^+
348 meson yields and their ratios in argon-nucleus interactions at the beam kinetic
349 energy of 3.2 AGeV. The results obtained are compared with the DCM-SMM,
350 UrQMD and PHSD models of nucleus-nucleus interactions and with the results
351 of other experiments in which nucleus-nucleus interactions at different energies
352 were studied.

353 The value of the inverse slope of the transverse momentum spectrum measured
354 for π^+ mesons is about 40 MeV in the forward rapidity range, rising to 90 MeV in
355 the central rapidity range. In general, the y dependence of the fitting results for π^+
356 mesons is consistent with the predictions of the models, but there is a tendency that
357 BM@N measures a flatter dependence of the slope values in the central rapidity
358 range compared to a rising dependence of the inverse slopes predicted by the
359 models.

360 The ratios of the K^+ to π^+ multiplicities show no significant dependence on
361 the mean number of participant nucleons of argon-nucleus collisions A_{part} . The
362 PHSD prediction is compatible with the BM@N result, whereas the DCM-SMM
363 and UrQMD models predict smooth rising of the K^+ to π^+ ratio with A_{part} .

364 The π^+ and K^+ multiplicities measured by BM@N and normalized on A_{part}
365 are found to be consistent with the rising energy dependence of the world data on
366 the production of π^+ and K^+ mesons measured for various colliding nuclei and
367 beam energies.

368 **Acknowledgments.** The BM@N Collaboration acknowledges support of the
369 HybriLIT of JINR, HPC Village project and HGPU group for the provided com-
370 putational resources.

371 **References**

- 372 [1] M. Kapishin (for the BM@N Collaboration), Eur. Phys. J. A52 (2016) no. 8,
373 213.
- 374 [2] J. Randrup and J. Cleymans, Phys. Rev. C 74 (2006) 047901.
- 375 [3] B. Friman, W. Nörenberg, and V.D. Toneev, Eur. Phys. J. A 3 (1998).
- 376 [4] NICA White Paper, Eur. Phys. J. A 52 (2016).

- 377 [5] BM@N Conceptual Design Report:
378 http://nica.jinr.ru/files/BM@N/BMN_CDR.pdf
- 379 [6] Ch. Fuchs, Prog. Part. Nucl. Phys. 56 (2006) 1-103.
- 380 [7] M. Kapishin (for the BM@N Collaboration), Nucl. Phys. A 982 (2019) 967-
381 970.
- 382 [8] M. Kapishin (for the BM@N Collaboration), SQM 2019 proceedings, 285
383 Springer Proc. Phys. 250 (2020) 21-27.
- 384 [9] BM@N project:
385 http://nica.jinr.ru/files/BM@N/BMN_project.pdf
- 386 [10] D. Baranov et al., JINST 12 (2017) no. 06, C06041 .
- 387 [11] V. Akishina and I. Kisel, J. Phys.: Conf. Ser. 599, 012024 (2015), I. Kisel,
388 Nucl. Instrum. Meth. A 566, 85 (2006).
- 389 [12] N. Amelin, K. Gudima, and V. Toneev, Sov. J. Nucl. Phys. 51, 1093 (1990).
- 390 [13] M. Baznat, A. Botvina, G. Musulmanbekov, V. Toneev, V. Zhezher, Phys.
391 Part. Nucl. Lett. 17 (2020) no. 3; arXiv: 1912.09277v.
- 392 [14] CERN Program Library, Long Writeup W5013, Geneva, CERN, 1993.
- 393 [15] <https://git.jinr.ru/nica/bmnroot>
- 394 [16] <http://garfieldpp.web.cern.ch/garfieldpp>
- 395 [17] D. Baranov et al., Phys. Part. Nucl. Lett. 15 (2018) no. 2, 148-156.
- 396 [18] S. A. Bass et al., Prog. Part. Nucl. Phys. 41 225 (1998).
- 397 [19] W. Cassing and E. L. Bratkovskaya, Nucl. Phys. A 831 (2009) 215-242.
- 398 [20] H. Angelov et al., P1-80-473, JINR, Dubna.
- 399 [21] G. Agakishiev et al., HADES Collaboration, Eur. Phys. J. A 47 (2011) 21.
- 400 [22] G. Agakishiev et al., HADES Collaboration, Phys. Rev. C 80 (2009) 025209.
- 401 [23] G. Agakishiev et al., HADES Collaboration, Phys. Rev. C 82 (2010) 044907.

- 402 [24] D. Best et al., FOPI Collaboration, Nucl. Phys. A 625 (1997) 307-324.
- 403 [25] N. Bastid et al., FOPI Collaboration, Phys. Rev. C 76 (2007) 024906.
- 404 [26] K. Piasecki et al., FOPI Collaboration, Phys. Rev. C 99 (2019) 1, 014904.
- 405 [27] M. Menzel et al., KaoS Collaboration, Phys. Lett. B 495 (2000) 26-32.
- 406 [28] A. Forster et al., KaoS Collaboration, Phys. Rev. C 75 (2007) 024906.
- 407 [29] K. Kanaki, PhD Thesis, Technische Universität Dresden, 2007.
- 408 [30] Yu. Kovalev et al., 2017 JINST 12 C07031; B. Topko et al., in IEEE Trans-
409 actions on Nuclear Science, vol. 69, no. 1, pp. 98-104, Jan. 2022; Topko,
410 B. L. et al., Phys. Part. Nuclei 53, 639–643 (2022); Yu. Topko et al., Nucl.
411 Instrum. Meth. A 1033, 166680 (2022) .
- 412 [31] A. Galavanov et al., EPJ Web Conf. 204 (2019) 07009; A. Galavanov et al.,
413 2020 JINST15 C09038.
- 414 [32] M. Kapishin et al., EPJ Web Conf., 173 (2018) 04008; E. Mazzucato, Nucl.
415 Phys. B 59 (1997) 174-181.
- 416 [33] V. Babkin et al., Nucl. Instrum. Meth. A 824, P.490–492 (2016); V. Babkin
417 et al., Proceedings of Science, 2014, Vol.213 (Proceedings of TIPP-2014),
418 P.289 .
- 419 [34] N. Kuzmin et al., Nucl. Instrum. Meth. A 916, P. 190–194 (2019) .
- 420 [35] K. Alishina et al., Phys. Part. Nucl., 53 (2022) no. 2, 470-475.
- 421 [36] P. Senger et al., J. Phys. G 25 (1999) R59-R131.
- 422 [37] J. Adamczewski-Musch et al., Eur. Phys. J. A 56 (2020) 259.
- 423 [38] Gazdzicki M. and Röhrich D., 1995 Z. Phys. C 65 215.
- 424 [39] Anikina et al., JINR Rapid Comm Dubna, 1 (1989) 12.
- 425 [40] Harris J. W. et al., 1987 Phys. Rev. Lett. 58 463.
- 426 [41] Pelte D. et al., 1997 Z. Phys. A 357 215.
- 427 [42] Wagner A. et al., 1998 Phys. Lett. B 420 20.

- 428 [43] Schwalb O. et al., 1994 Phys. Lett. B 321 20.
- 429 [44] Harris J. W. et al., 1985 Phys. Lett. B 153 377.
- 430 [45] T. Abbott et al. (E-802 Collaboration), Phys. Rev. C 50 (1993) 1024.
- 431 [46] J. Bachler et al., Phys. Rev. Lett. 72 (1994) 1419.
- 432 [47] Jacobs P. and NA49 Collaboration 1997 Proc. of the 3rd Int. Conf. on the
433 Physics and Astrophysics of the Quark Gluon Plasma (Jaipur, India) (Delhi:
434 Narosa).
- 435 [48] W. Reisdorf et al. (FOPI Collaboration), Nucl. Phys. A 781, 459 (2007).
- 436 [49] A.R. Wolf et al. (TAPS Collaboration), Phys. Rev. Lett. 80, 5281 (1998).
- 437 [50] R. Averbeck et al., Phys. Rev. C 67, 024903 (2003).
- 438 [51] J.L. Klay et al. (E895 Collaboration), Phys. Rev. C 68, 054905 (2003).
- 439 [52] R. Barth et al. Phys. Rev. Lett. 78 (1997), p. 4007.
- 440 [53] L. Ahle et al. (E802 Collaboration), Phys. Rev. C 60, 044904 (1999).
- 441 [54] L. Ahle et al. (E802 Collaboration), Phys. Rev. C 58, 3523 (1998).
- 442 [55] Afanasiev S. V. et al., Phys. Rev. C. 66 054902 (2002).

Table 2: 1) Extrapolation coefficients for π^+ and K^+ meson multiplicities from the measured range to the entire kinematical range. The coefficients are averaged over predictions of the DCM-SMM, PHSD, UrQMD models. Uncertainties are taken as the maximal differences of the predictions of the models from the averaged values. 2) Number of participant nucleons from predictions of the DCM-SMM model. 3) Inclusive cross sections for inelastic Ar+A interactions.

3.2 AGeV argon beam	Ar+C	Ar+Al	Ar+Cu	Ar+Sn	Ar+Pb
Extrap. coeff. for π^+	3.25 ± 0.18	3.73 ± 0.13	4.45 ± 0.07	5.12 ± 0.26	5.91 ± 0.55
Extrap. coeff. for K^+	2.81 ± 0.66	3.02 ± 0.67	3.34 ± 0.65	3.7 ± 0.58	4.1 ± 0.43
$A_{\text{part, DCM-SMM}}$	14.8	23.0	33.6	48.3	63.6
$\sigma_{\text{inel, mb [29]}}$	1470 ± 50	1860 ± 50	2480 ± 50	3140 ± 50	3940 ± 50

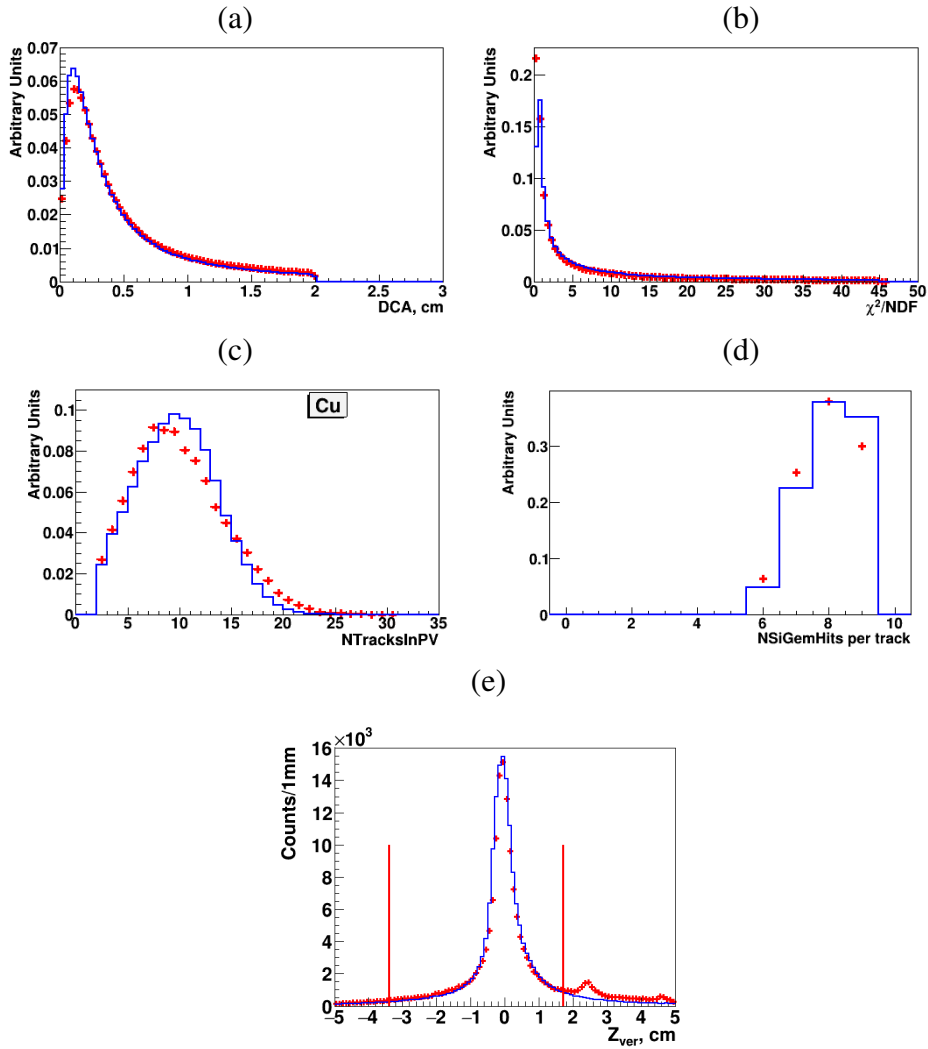


Figure 7: Ar+A interactions at 3.2 AGeV : comparison of the experimental distributions (red crosses) and reconstructed Monte Carlo GEANT distributions of events generated with the DCM-SMM model (blue lines): DCA; χ^2/NDF of reconstructed tracks; number of tracks reconstructed in the primary vertex; number of hits per track reconstructed in 3 forward silicon and 6 GEM detectors; primary vertices along the Z axis for data and simulated events (vertical lines limit the Z region taken for the data analysis).

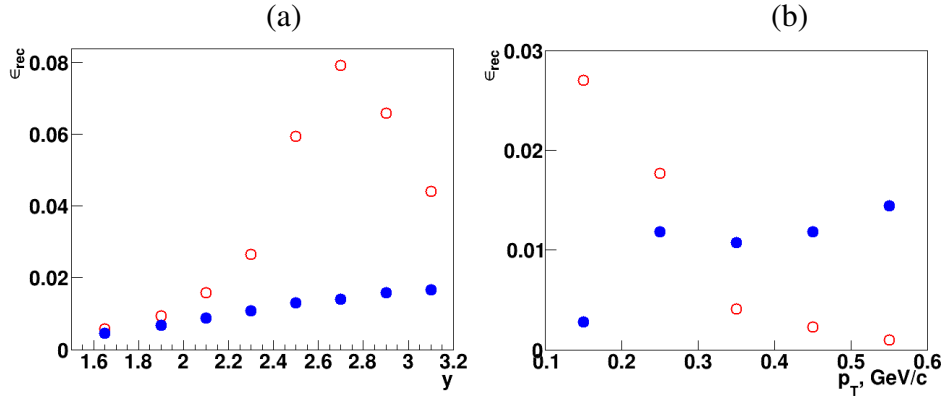


Figure 8: Reconstruction efficiency of π^+ detected in ToF-400 (open red circles) and ToF-700 (full blue circles), calculated as a product of the geometrical acceptance, detector efficiency and efficiency of kinematic and spatial cuts in bins of the rapidity y in the laboratory frame (a) and in bins of p_T (b). The results are shown for π^+ mesons produced in Ar+Sn interactions.

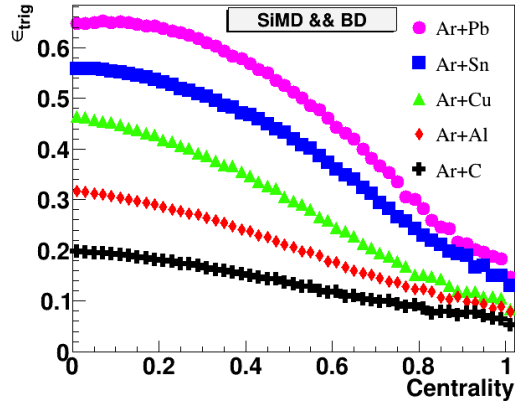


Figure 9: Trigger efficiency for interactions of the argon beam with various targets (C, Al, Cu, Sn, Pb) as a function of the event centrality estimated from the simulation.

Table 3: π^+ and K^+ meson multiplicities measured in Ar+C, Al, Cu, Sn, Pb interactions at the argon beam energy of 3.2 AGeV. The first error given is statistical, the second error is systematic. The third error given for the full π^+ and K^+ multiplicities is the model uncertainty.

3.2 AGeV argon beam	Ar+C	Ar+Al	Ar+Cu	Ar+Sn	Ar+Pb
Measured π^+ mult. N_{π^+}	$0.42 \pm 0.008 \pm 0.045$	$1.00 \pm 0.01 \pm 0.07$	$1.14 \pm 0.01 \pm 0.08$	$1.28 \pm 0.01 \pm 0.09$	$1.25 \pm 0.01 \pm 0.08$
Measured K^+ mult. $N_{K^+}/10^{-2}$	$1.59 \pm 0.29 \pm 0.65$	$3.90 \pm 0.28 \pm 0.61$	$4.17 \pm 0.21 \pm 0.66$	$5.60 \pm 0.22 \pm 0.75$	$5.10 \pm 0.22 \pm 0.92$
Full π^+ mult. $N_{\pi^+}^{tot}$	$1.365 \pm 0.026 \pm 0.146 \pm 0.08$	$3.73 \pm 0.04 \pm 0.26 \pm 0.13$	$5.07 \pm 0.04 \pm 0.36 \pm 0.08$	$6.55 \pm 0.05 \pm 0.46 \pm 0.33$	$7.39 \pm 0.06 \pm 0.47 \pm 0.69$
Full K^+ mult. $N_{K^+}^{tot}/10^{-2}$	$4.47 \pm 0.81 \pm 1.83 \pm 1.05$	$11.8 \pm 0.9 \pm 1.8 \pm 2.6$	$13.9 \pm 0.7 \pm 2.2 \pm 2.7$	$20.7 \pm 0.8 \pm 2.8 \pm 3.3$	$20.9 \pm 0.9 \pm 3.8 \pm 2.2$
$N_{K^+}/N_{\pi^+}/10^{-2}$ Measured range	$3.79 \pm 0.69 \pm 1.52$	$3.90 \pm 0.28 \pm 0.55$	$3.66 \pm 0.19 \pm 0.53$	$4.39 \pm 0.18 \pm 0.51$	$4.11 \pm 0.18 \pm 0.68$
$N_{K^+}^{tot}/N_{\pi^+}^{tot}/10^{-2}$, Full kin. range	$3.27 \pm 0.6 \pm 1.38 \pm 0.79$	$3.16 \pm 0.23 \pm 0.54 \pm 0.71$	$2.75 \pm 0.14 \pm 0.48 \pm 0.54$	$3.16 \pm 0.13 \pm 0.48 \pm 0.52$	$2.83 \pm 0.12 \pm 0.54 \pm 0.39$
K^+ inv. slope T_0 , MeV, Meas. range	$67 \pm 12 \pm 12$	$80 \pm 7 \pm 5$	$81 \pm 5 \pm 5$	$81 \pm 5 \pm 4$	$78 \pm 5 \pm 4$

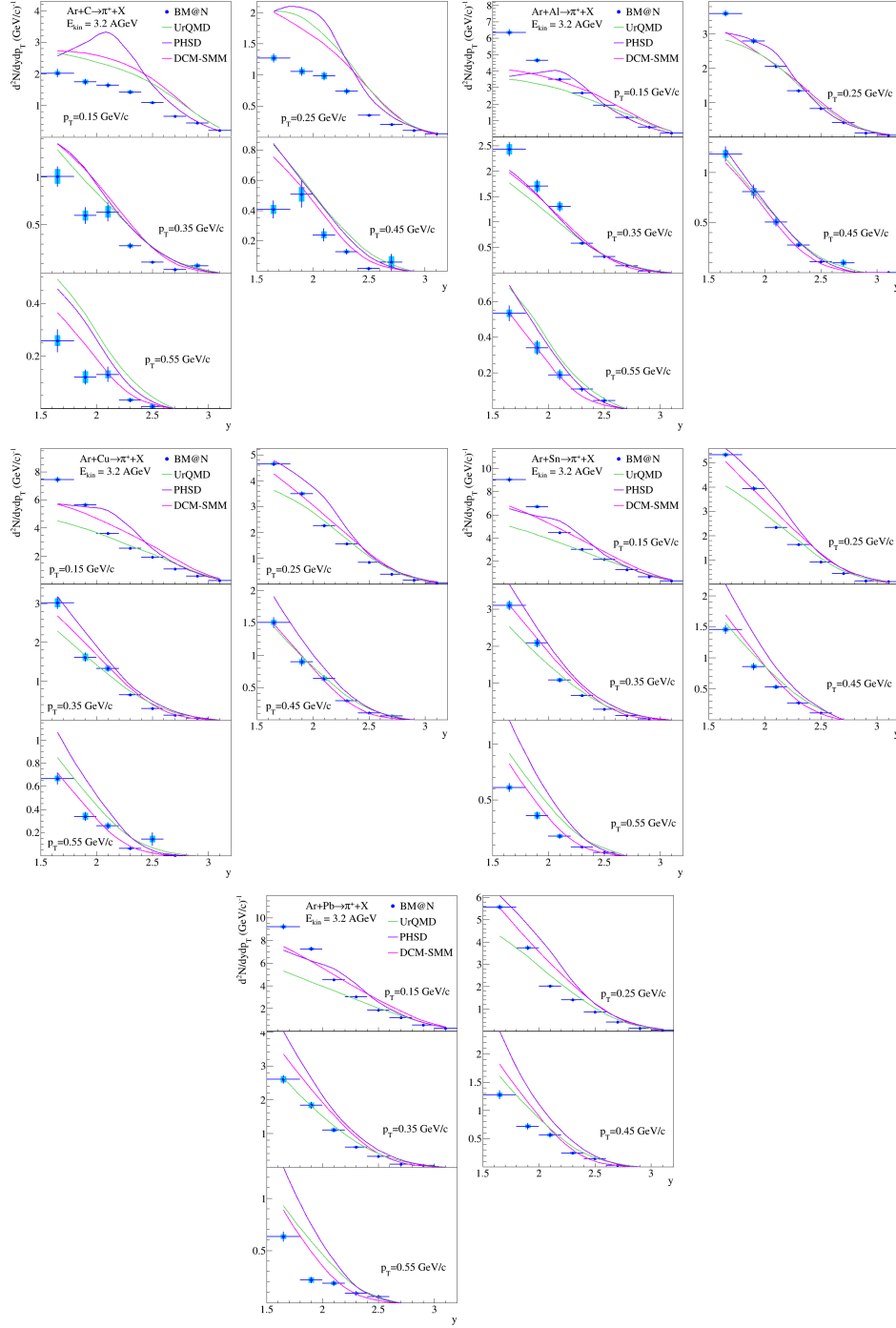


Figure 10: Rapidity spectra (y) of π^+ mesons produced in Ar+C, Al, Cu, Sn, Pb interactions at the argon beam energy of 3.2 AGeV. The results are given for bins of π^+ meson transverse momentum. The error bars represent the statistical errors, the boxes show the systematic errors. The predictions of the DCM-SMM, UrQMD and PHSD models are shown as rose, green and magenta lines.

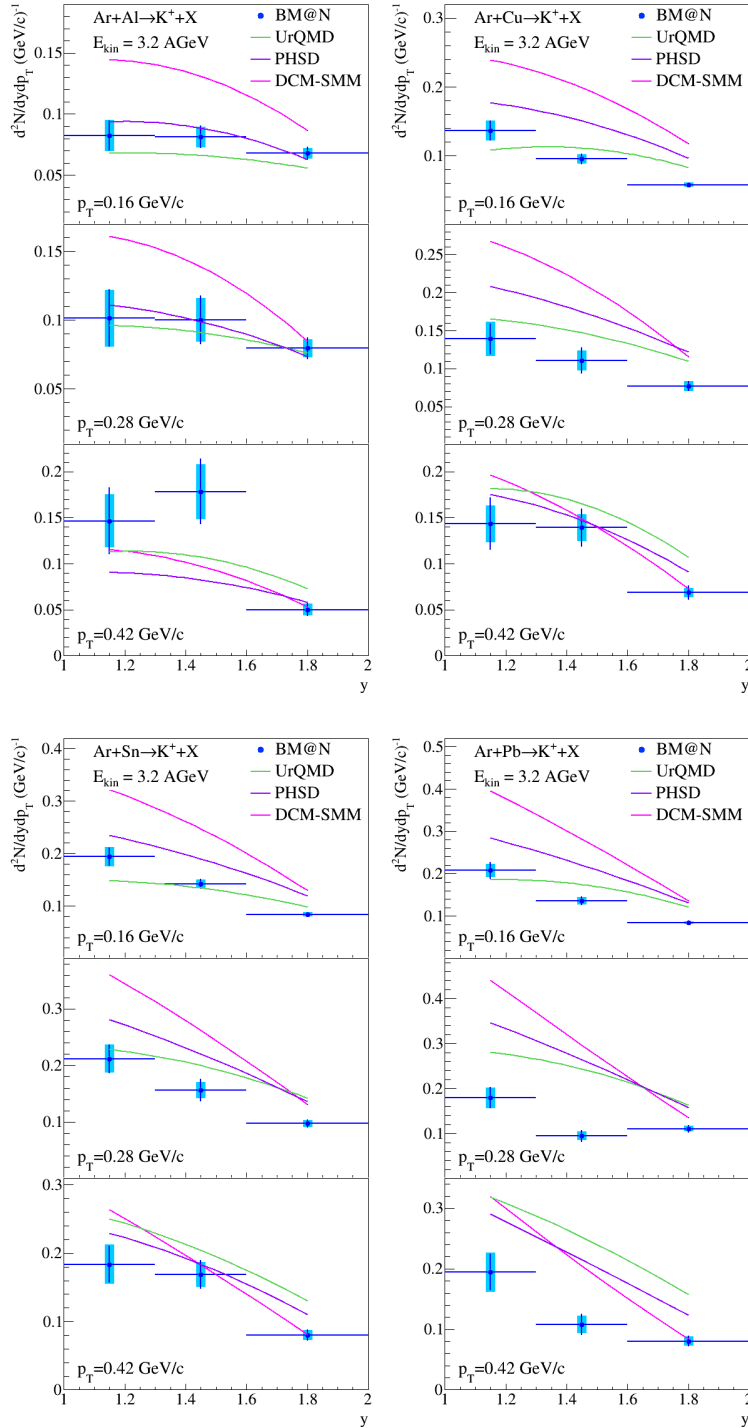


Figure 11: Rapidity spectra (y) of K^+ mesons produced in Ar+Al, Cu, Sn, Pb interactions at the argon beam energy of 3.2 AGeV. The results are given for bins of K^+ meson transverse momentum. The error bars represent the statistical errors, the boxes show the systematic errors. The predictions of the DCM-SMM, UrQMD and PHSD models are shown as rose, green and magenta lines.

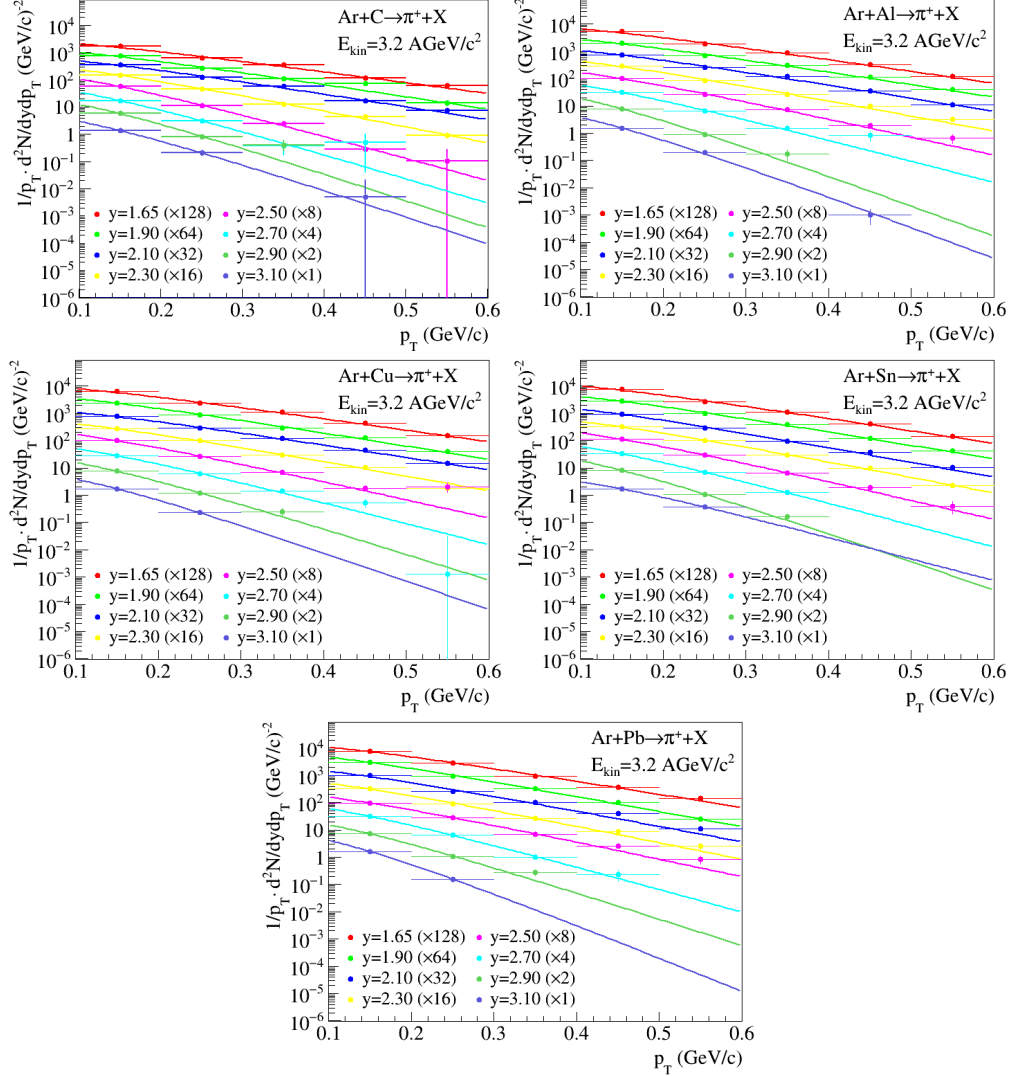


Figure 12: Transverse momentum spectra (p_T) of π^+ mesons produced in Ar+C, Al, Cu, Sn, Pb interactions at the argon beam energy of 3.2 AGeV. The results are given for bins of π^+ meson rapidity. The lines represent the results of the parameterization described in the text.

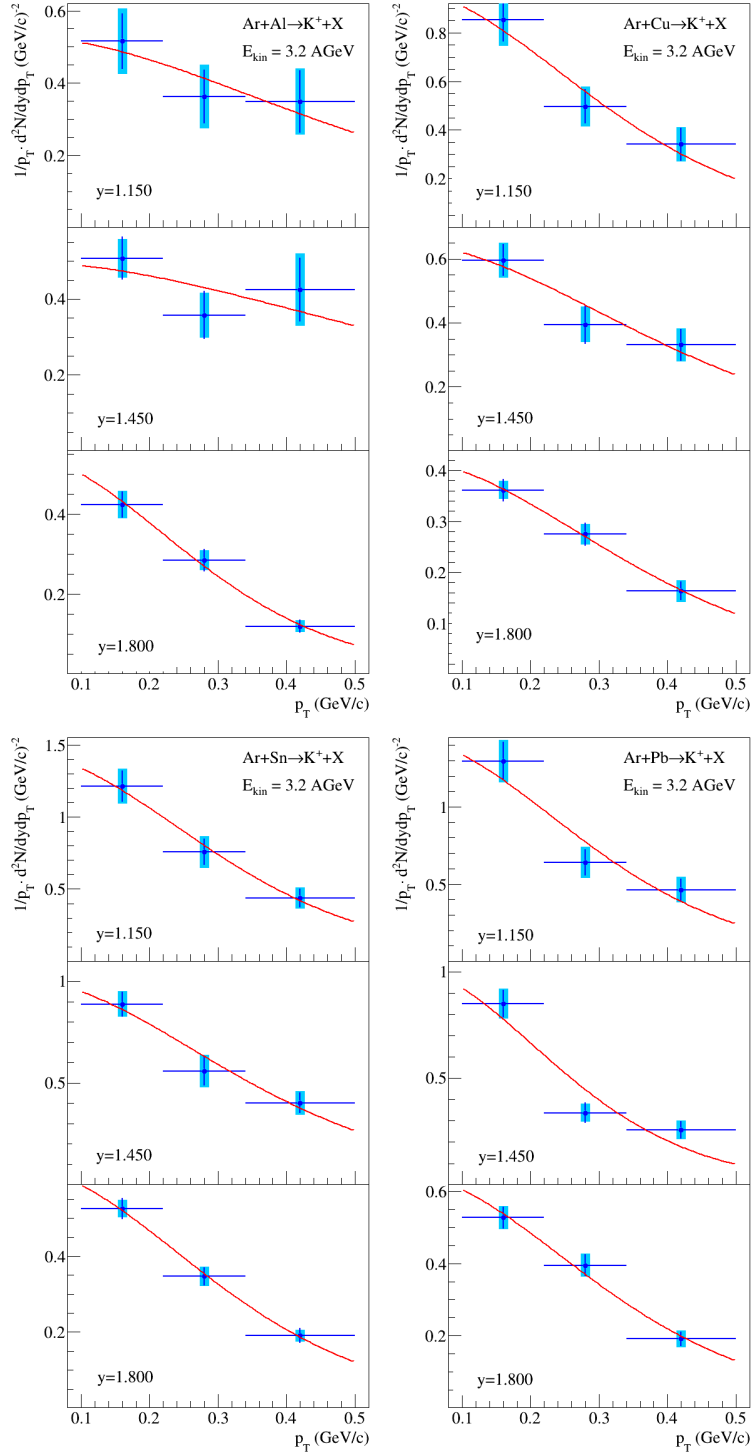


Figure 13: Transverse momentum spectra (p_T) of K^+ mesons produced in Ar+Al, Cu, Sn, Pb interactions at the argon beam energy of 3.2 AGeV. The results are given for three bins of K^+ meson rapidity. The error bars represent the statistical errors, the boxes show the systematic errors. The lines represent the results of the parameterization described in the text.

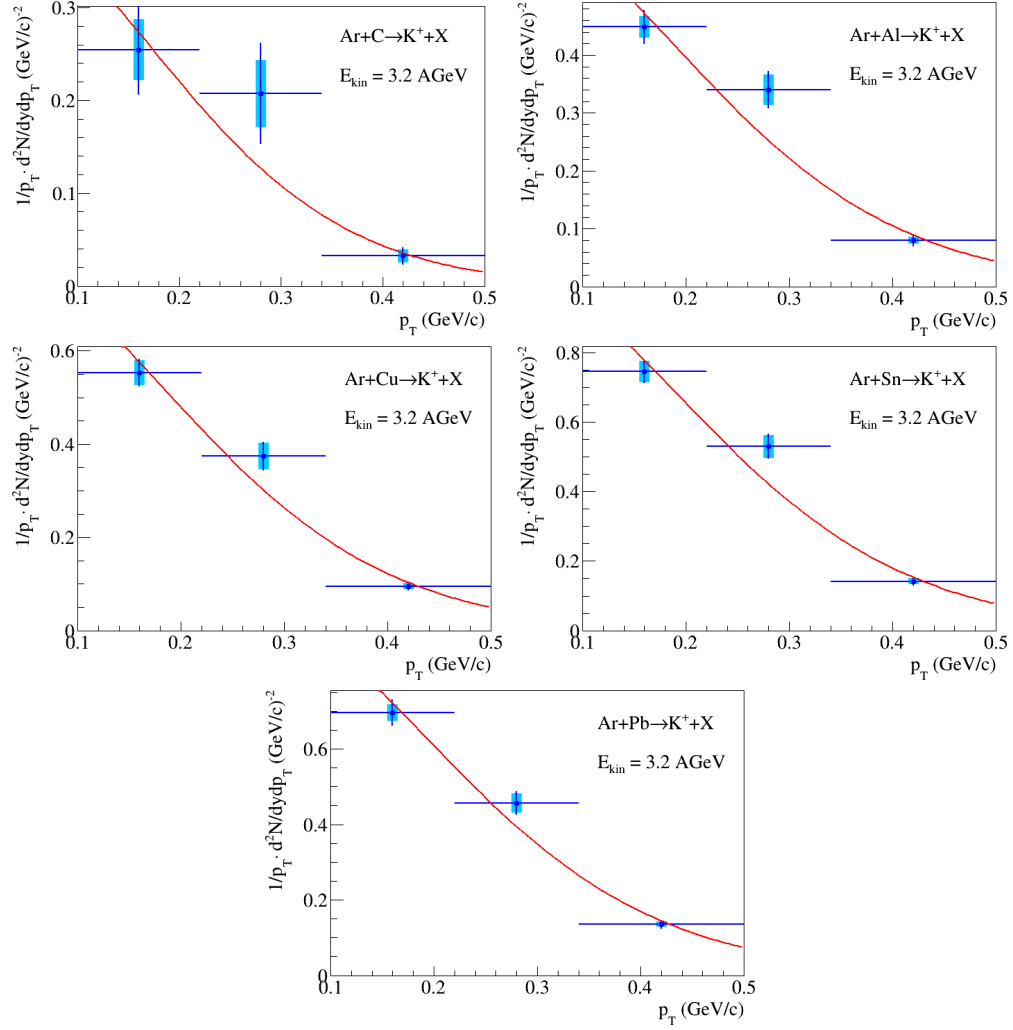


Figure 14: Transverse momentum spectra (p_T) of K^+ mesons produced in Ar+C, Al, Cu, Sn, Pb interactions at the argon beam energy of 3.2 AGeV. The results are given for the measured K^+ meson rapidity range. The error bars represent the statistical errors, the boxes show the systematic errors. The lines represent the results of the parameterization described in the text.

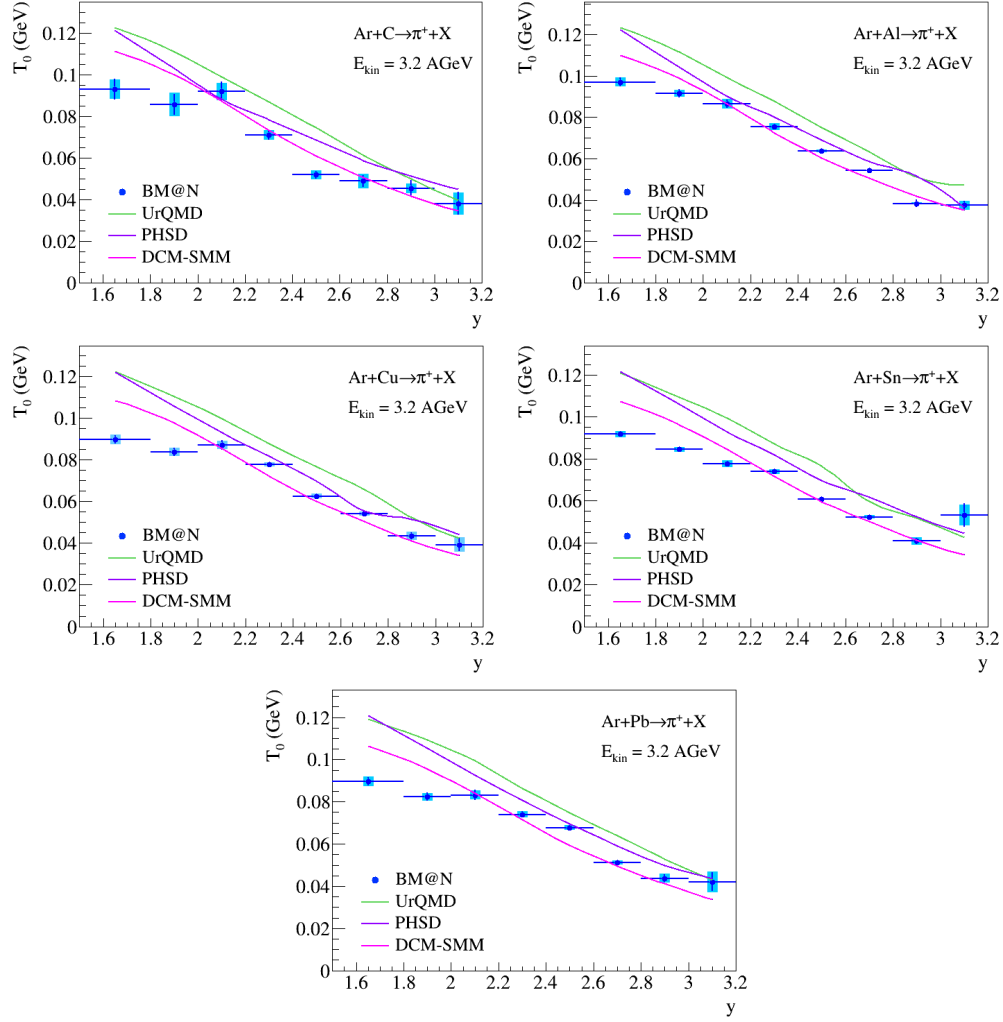


Figure 15: Rapidity y dependence of the inverse slope T_0 determined from the fits of the π^+ p_T spectra in Ar+C, Al, Cu, Sn, Pb interactions. The error bars represent the statistical errors, the boxes show the systematic errors. The predictions of the DCM-SMM, UrQMD and PHSD models are shown as rose, green and magenta lines.

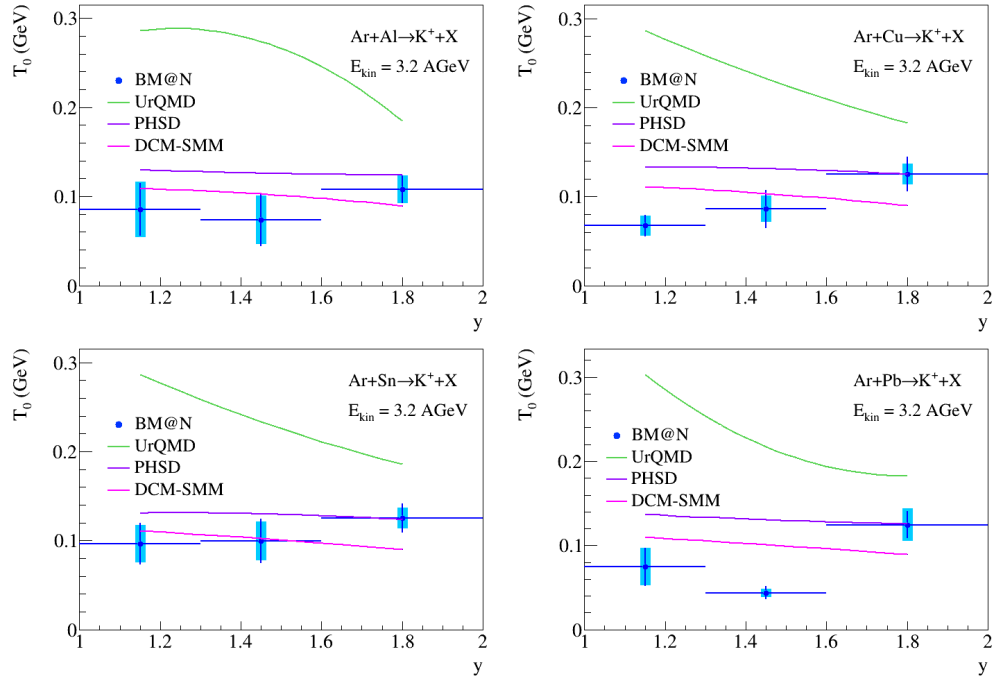


Figure 16: Rapidity y dependence of the inverse slope T_0 extracted from the fits of the K^+ p_T spectra in Ar+Al, Cu, Sn, Pb interactions. The error bars represent the statistical errors, the boxes show the systematic errors. The predictions of the DCM-SMM, UrQMD and PHSD models are shown as rose, green and magenta lines.

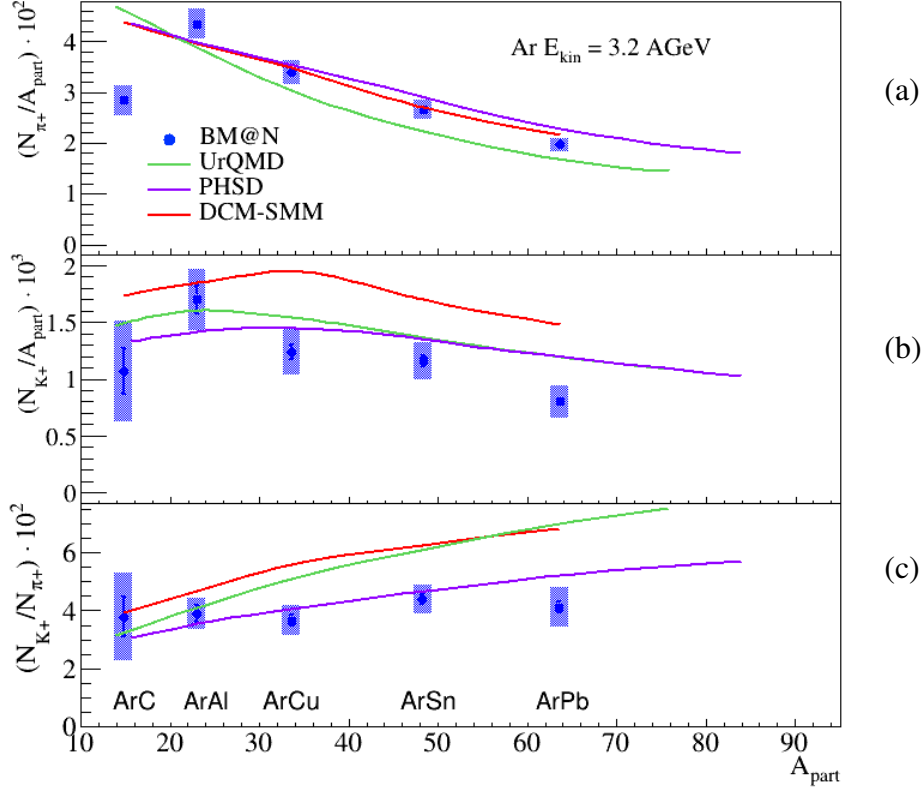


Figure 17: Ratios of the π^+ (a) and K^+ (b) multiplicities to the number of participant nucleons and ratios of the K^+ to π^+ multiplicities (c) in the measured kinematical range in Ar+C, Al, Cu, Sn, Pb interactions. The error bars represent the statistical errors, the blue boxes show the systematic errors. The BM@N results are compared with predictions of the DCM-QGSM, UrQMD and PHSD models for argon-nucleus interactions shown as red, green and magenta lines.

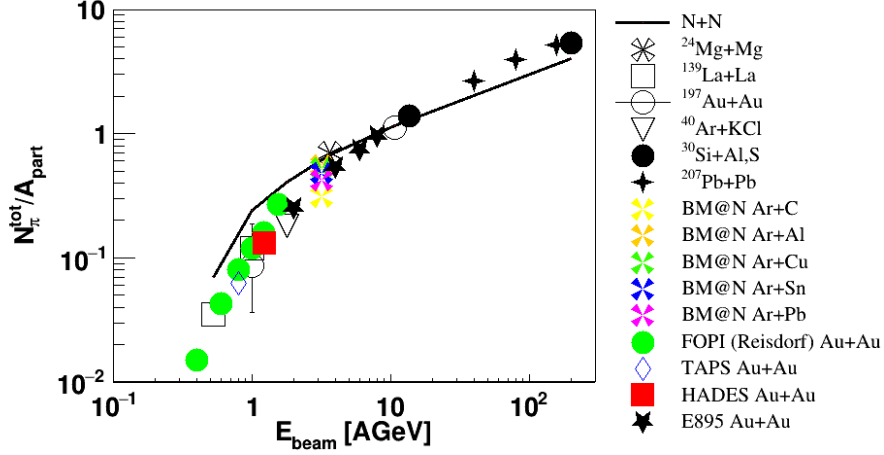


Figure 18: Pion multiplicity N_{π}^{tot} per the mean number of participant nucleons A_{part} shown as a function of the beam kinetic energy E_{beam} . The BM@N results are compared with the world measurements (references in the text).

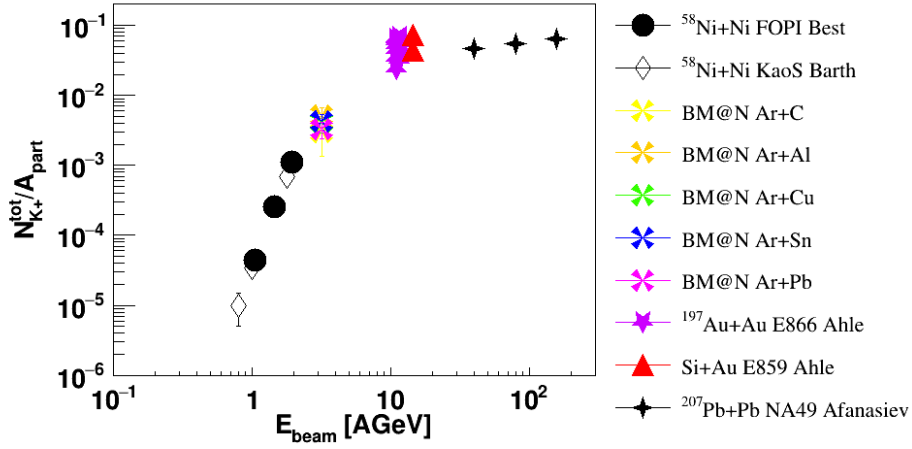


Figure 19: K^+ multiplicity per the mean number of participant nucleons A_{part} shown as a function of the beam kinetic energy E_{beam} . The BM@N results are compared with the world measurements (references in the text).